Project report for final year project in Physics & Astronomy

The formation of Einstein-Dirac solitons: a phase transition in the early universe

Matriculation Number: 160018530

Module: PH5103 MPhys Theoretical Physics

Science is often highly collaborative. Please clarify here which parts of the work reported have been done by you and which parts include the work of others. For example, this might include provision of simulation or analysis codes which you utilised or modified, provision of experimental data to analyse, collaborations with others in performing new measurements, if you built up things from scratch in your project or started from pre-existing setups, and others. Providing this information helps clarify the scope and focus of your project work.

All the project work has been done by me.

Abstract

Finster, Smoller and Yau [*Phys. Rev.* D **59**, 104020 (1999)] found static, spherically symmetric localized solutions to the Einstein-Dirac equations called Einstein-Dirac solitons (EDS). This work considers a modified version of the Einstein-Dirac system that takes into account a non-zero cosmological constant and a uniform matter background. We show that EDS occur in this context, and we qualitatively identify a localization regime bounded above and below by the cosmological constant. The formation of EDS as a phase transition between a state of uniform energy density and one where fermions condense out in localized structures constitutes a promising analogue to particle generation in the early universe. We introduce a model that utilizes EDS to reproduce a uniform matter background and that can be used to investigate their formation.

Dedication

To my mother Ornella, who always supported me and believed in me in the most difficult times. To my grandfather Michele and grandmother Margherita, who I love dearly and always keep in my heart.

Acknowledgements

I would like to thank my supervisors, Keith and Chris, for their help and support throughout this project.

Contents

1. Introduction

1.1 What is quantum gravity and why is it interesting?

One of the biggest challenges theoretical physics has ever faced is posed by the apparent incompatibility of the four fundamental forces of nature. Three of them - electromagnetic, strong and weak interaction - are formulated as quantum field theories, and are beautifully embedded in the theory of the Standard Model (SM). The fourth one, gravity, is described by Einstein's theory of General Relativity (GR). Both theories have been thoroughly tested experimentally and both contributed to critical discoveries for the advancement of physics [1, 2, 3, 4].

However, all attempts to unify GR and the SM in a consistent formulation of quantum gravity (QG) have so far been unsuccessful [5]. Furthermore, the effects of the interplay between gravity and quantum mechanics are thought to become relevant at the Planck length

$$l_p = \sqrt{\frac{\hbar G}{c^3}} \sim 10^{-35}\, m, \tag{1.1}$$

far below the probing limits of the most advanced particle accelerators. Experimental verification of predictions from existing QG models, such as string theory and loop quantum gravity, is therefore impossible.

Nonetheless, the formulation of a consistent theory of QG is one of the most important areas of research in contemporary physics. It would pose a fundamental building block towards the unification of all interactions of nature in a coherent mathematical framework. Furthermore, it would give interesting insights in the physics of Planck scale processes, such as the evolution of black holes [6, 7]; spacetime singularities [8, 9]; the geometry of spacetime at the Planck scale and associated quantum foam [10]; initial conditions in early cosmology [11, 12].

1.2 The Einstein-Dirac system: an overview

A promising way to investigate QG involves combining a classical treatment of gravity and a quantum treatment of matter. This approximation, adopted for the first time by Brill and Wheeler in 1957 to describe neutrinos [13], takes the name of semi-classical QG. One important such model is the Einstein-Dirac (ED) system, which couples Einstein's field equations to the Dirac equation. It was formulated by Lee and Pang in 1987, who found gravitationally localized states in the context of soliton stars and black holes [14]. Two years later, in 1990, Finster, Smoller and Yao (FSY) considered a couple of fermions in a singlet state and discovered numerically exact solutions: Einstein - Dirac solitons (EDS) [15]. While the term soliton is an umbrella-term for a wide variety of mathematical objects and physical phenomena [16, 17], it is used here to highlight the fact that these solutions are solitary, stationary, localized solutions to nonlinear differential equations, with dispersion balanced by the nonlinearity.

The physics they display sheds light on the interaction between gravity and quantum mechanics. While the former compresses the fermions together, the latter pushes them apart via the Heisenberg uncertainty principle, preventing the collapse into a black hole. This mechanism causes the system to localize in a standing wavepacket which bounces off its self-generated gravitational well, resulting in a self-trapping effect.

Further developments expanded the ED system to include the electromagnetic force [18], an SU(2) Yang-Mills field [19], and the Higgs field [20]. Large particle numbers and strong gravitational regimes have also been investigated [21, 22]. In all these contexts, solitonic solutions were found to exist. EDS analogues occur also in the bosonic case, where they take the name of boson stars for spin-0 and Proca stars for spin-1 particles [23, 24]. Notably, the existence of black holes has also been investigated in this context [25, 26, 27].

1.3 Motivation & structure

The project aligns with the above line of research. In particular, our work has been informed by the question of how EDS behave when embedded in a uniform matter background. This scenario is interesting to consider because it mimics early universe conditions. The time-span

between 10^{-12} and 10^{-5} seconds after the Big Bang is called the Quark epoch. In this era, the universe was filled by the Quark-Gluon Plasma, a soup of unbound elementary particles in thermal equilibrium [28]. As the universe expanded and cooled, the energy density dropped, allowing hadrons to form. Eventually, it became too low to sustain heavy particles such as the tau lepton and top quark, and the lighter ones became more prevalent. Particle formation was therefore driven by the rapid decrease of energy density.

We develop a model to study an analogous system where space is filled by EDS in different density regimes. At extremely low densities, the fermions are infinitely far away and do not interact with one another. In this limit, they are effectively an isolated system analogous to the one considered by FSY, and solitonic solutions are expected to arise. However, in the high density limit, the matter fields overlap with each other, generating an effective uniform matter background. Whether solitons form or not when embedded in such background is an open question. If they do not, then there must be a phase transition occurring between two distinct states: one where the environment is filled with uniform matter, and one where fermions condense out to form solitons localized by their own self-gravity. The transition would be driven by the variation of the energy density, analogously to how particle formed in early universe conditions.

The report is organised as follows. In Section 2, we consider a new formulation of the Einstein-Dirac system with a non-zero cosmological constant, in order to account for cosmological effects. We then analyse mathematically the behaviour of the system in a number of limit cases and solve the relevant Einstein equations. This will provide analytical guidance to assess the accuracy of our numerical results. In Section 3, we detail the methods used to solve the ED system numerically. To test the efficacy of our algorithm, we reproduce the FSY ground state EDS. We then proceed to show that solitonic solutions exist when a non-zero cosmological constant is taken into account, and we qualitatively identify a localization regime that is bound by this parameter. Furthermore, we show that EDS occur in the presence of a uniform matter background. In Section 4, we introduce a model that utilizes EDS to reproduce a uniform matter background and that might be used to investigate their formation. The scope of the model is illustrated and the underlying methods detailed. Results are presented and limitations are

discussed. Finally, Section 5 provides a summary and considers possible further developments to this work.

2. The Einstein-Dirac system

2.1 Derivation

This section follows [15, 22] and details how to obtain a modified version of the ED equations which accounts for a non-zero cosmological constant. A full derivation of the ED equations lies beyond the scope of this project.

We consider a system of N fermions, where we achieve spherical symmetry by filling shells of $N = 2j + 1$ particles with zero net angular momentum, where j is the total (spin+orbital) angular momentum and N is even. This admits the existence of solutions which are functions of the radial coordinate only. We work in natural units $c = \hbar = G = 1$, which will allow numerical results to be presented with the radial coordinate expressed in Planck length units l_p.

The Einstein field equations in the presence of a non-zero cosmological constant are

$$G_{\mu\nu} + \Lambda g_{\mu\nu} = R_{\mu\nu} + \left(\Lambda - \frac{1}{2}R\right) g_{\mu\nu} = -8\pi T_{\mu\nu}. \tag{2.1}$$

Raising one index, we get

$$G^{\mu}_{\nu} + \Lambda \delta^{\mu}_{\nu} = -8\pi T^{\mu}_{\nu}. \tag{2.2}$$

Under the assumption of static, symmetric spacetimes, we use the following metric

$$g_{\mu\nu} = diag\left(-\frac{1}{T^2}, +\frac{1}{A}, +r^2, +r^2 \sin\theta^2\right), \tag{2.3}$$

where $T = T(r)$ and $A = A(r)$ are the metric fields, respectively the time-dilation and length-contraction factor. To calculate the Einstein tensor components from this metric, we use the

Mathematica package GRQUICK. The components are

$$G_0^0 = -\frac{1}{r^2} + \frac{A}{r^2} + \frac{A'}{r}, \tag{2.4}$$

$$G_1^1 = -\frac{1}{r^2} + \frac{A}{r^2} - \frac{2AT'}{rT}, \tag{2.5}$$

$$G_2^2 = G_3^3 = \frac{A'}{2r} - \frac{AT'}{rT} - \frac{A'T'}{2T} + \frac{2AT'^2}{T^2} - \frac{AT''}{T}. \tag{2.6}$$

All the other components vanish, which is to be expected since the metric is diagonal.

The mixed stress-energy tensor is

$$T_\nu^\mu = \frac{1}{r^2} diag\Bigg(N\omega T^2(\alpha^2+\beta^2), -N\omega T^2(\alpha^2+\beta^2) + \frac{N^2\sigma T}{r}\alpha\beta + NmT\left(\alpha^2-\beta^2\right), \\ -\frac{NT}{r}\alpha\beta, -\frac{NT}{r}\alpha\beta\Bigg). \tag{2.7}$$

The two components of the Dirac equation for the ED system are

$$\sqrt{A}\alpha' = \frac{\sigma N}{2r}\alpha - (\omega T + m)\beta, \tag{2.8}$$

$$\sqrt{A}\beta' = -\frac{\sigma N}{2r}\beta + (\omega T - m)\alpha, \tag{2.9}$$

where $\alpha = \alpha(r)$ and $\beta = \beta(r)$ are respectively the particle-like and hole-like components of the Dirac spinor, which will be referred to as fermion fields. ω is the fermion frequency, m is the fermion mass and $\sigma = \pm 1$ is the parity of the solution. We note that describing quantum mechanical effects via the Dirac equation instead of via a second quantisation approach consists of an approximation intrinsic to the ED system.

We write out the components of (2.2) by combining (2.4) - (2.6) with (2.7):

$$rA' + A - 1 + \Lambda r^2 = -8\pi N\omega T^2(\alpha^2+\beta^2), \tag{2.10}$$

$$2rA\frac{T'}{T} - A + 1 - \Lambda r^2 = -8\pi\left(N\omega T^2(\alpha^2+\beta^2) - \frac{N^2\sigma}{r}T\alpha\beta - NmT(\alpha^2-\beta^2)\right), \tag{2.11}$$

$$\left(-\frac{A'}{2r}+\frac{AT'}{rT}+\frac{A'T'}{2T}-\frac{2AT'^2}{T^2}+\frac{AT''}{T}\right)r^2+\Lambda r^2=-\frac{8\pi N}{r}T\alpha\beta, \tag{2.12}$$

where the $\phi\phi$ and $\theta\theta$ components are equal to each other by spherical symmetry. The equations (2.8) - (2.11) compose the ED system of equations. Note that when $\Lambda = 0$, (2.12) is implied by (2.8) - (2.11) [15]. Thus, to infer this conclusion for $\Lambda \neq 0$, it suffices to show that the LHS of (2.10) and (2.11) imply the LHS of (2.12), which can be done by direct substitution.

2.2 Asymptotic behaviour of the metric

Before proceeding to solve the ED system numerically, we consider the asymptotic behaviour that the equations display in a number of scenarios and solve the relevant Einstein equations. This will provide analytical guidance to check the consistency of the numerical solutions presented in Section 3.

Far away from the matter sources at the origin, the fermion fields α and β vanish. In the FSY case of $\Lambda = 0$, spacetime is expected to be asymptotically Minkowskian (i.e, flat). The presence of non-zero Λ changes this behaviour. By setting $\alpha = \beta = 0$, (2.10) and (2.11) become

$$rA' = 1 - A - \Lambda r^2, \tag{2.13}$$

$$2rA\frac{T'}{T} = A - 1 + \Lambda r^2. \tag{2.14}$$

Consider (2.13). By moving A to the RHS and recognising the expansion of $d(Ar)/dr$, we can integrate both sides and rearrange:

$$A(r) = 1 + \frac{c_1}{r} - \frac{\Lambda r^2}{3}. \tag{2.15}$$

Solving (2.14) with the integrating factor method (see Appendix A) yields

$$T(r) = \frac{c_2}{\sqrt{1 + c_1/r - \Lambda r^2/3}} = \frac{c_2}{\sqrt{A}}. \tag{2.16}$$

By setting $c_1 = -2M$ and $c_2 = 1$, we recover the Schwarzchild-De Sitter metric

$$ds^2 = -\left(1 - \frac{2M}{r} - \frac{\Lambda}{3}r^2\right)dt^2 + \left(1 - \frac{2M}{r} - \frac{\Lambda}{3}r^2\right)^{-1} dr^2 + r^2 d\theta^2 + r^2 \sin\theta^2 d\phi^2, \qquad (2.17)$$

where $\Lambda > 0$, and where M is the ADM mass of a point mass embedded in a uniformly curved spacetime [29]. If $\Lambda < 0$, (2.17) is called Schwarzchild-anti-De Sitter metric. Far away from the origin, we expect the metric fields solutions to the ED system to match onto this metric.

Where A crosses zero and T becomes complex, the metric has an horizon. Only the region bounded by horizons is physically meaningful for our solutions. To find where these occur, we can make use of the fact that A is a cubic and express it as

$$A(r) = \frac{(r - r_{sc})(r - r_+)(r - r_-)}{r}. \qquad (2.18)$$

Since r is the radial coordinate, only real positive roots are physical. For $\Lambda > 1/(9M^2)$ there are no positive real roots. For $0 < \Lambda < 1/(9M^2)$ there are two positive real roots, while for $\Lambda < 0$, there is one positive real root (see Appendix B). Both these two cases have a black hole horizon occurring at a small positive radius r_{sc} due to the point mass at the origin. For $0 < \Lambda < 1/(9M^2)$, the second real root corresponds to an horizon at some large radius r_+ where the $-\Lambda/3r^2$ term is dominant. This second horizon takes the name of cosmological horizon. In the extreme case of $\Lambda = 1/(9m^2)$, the black hole and cosmological horizons are superposed [29].

If $\Lambda = 0$, (2.17) reduces to the usual Schwarzchild metric, while (2.15) and (2.16) become

$$A(r) = 1 - \frac{2M}{r} = \frac{1}{T^2}, \qquad (2.19)$$

where $r_{sc} = 2M$ corresponds to the usual Schwarzchild radius.

If $c_1 = -2M = 0$, (2.16) gives the vacuum solutions to the Einstein equations. Although spacetime is empty, it presents a uniform constant curvature due to the cosmological constant. Computing the Ricci scalar with GRQUICK yields $R = 4\Lambda$, a result general to all vacuum Einstein equations [30]. In this case, if $\Lambda > 0$, the cosmological horizon lies at $r_+ = \sqrt{\Lambda/3}$.

In the presence of a uniform matter background, we have a uniform density ρ and uniform

isotropic pressure P filling all of spacetime. The stress-energy tensor of such background is equivalent to that of a perfect fluid [31], which gives

$$rA' = 1 - A - (\Lambda + 8\pi\rho)r^2, \tag{2.20}$$

$$2rA\frac{T'}{T} = A - 1 + (\Lambda - 8\pi P_r)r^2. \tag{2.21}$$

Note the similarity of (2.20) to (2.13). We can regard the $8\pi\rho$ term as a finite correction to the effect of the cosmological constant, which allows to write the solution straightforwardly

$$A(r) = 1 - \frac{2M}{r} - \frac{1}{3}(\Lambda + 8\pi\rho)r^2, \tag{2.22}$$

where we have directly identified the integration constant as $-2M$. This is the solution for a point mass embedded in uniform matter of density ρ. We could not find a close analytical solution for T in (2.21); Mathematica's DSolve gives a solution, albeit a rather cumbersome and unusable one.

However, by restricting our solutions to scenarios where no point masses are present, so that

$$A(r) = 1 - \frac{1}{3}(\Lambda + 8\pi\rho)r^2, \tag{2.23}$$

we can solve (2.21) via the integrating factor method (see appendix A). We find

$$T(r) = c_3 A^{\delta}, \tag{2.24}$$

where

$$\delta = \frac{2\pi\rho(1 + 3w) - \Lambda/2}{\Lambda + 8\pi\rho}, \tag{2.25}$$

$$w = \frac{P}{\rho}, \tag{2.26}$$

c_3 is an integration constant and (2.26) is the equation of state of the background. Since the cosmological constant, the energy density and the pressure all come into play in determining

the curvature of spacetime, it is sometimes useful to define the following "effective" quantities

$$\rho' = \rho + \frac{\Lambda}{8\pi}, \qquad P' = P - \frac{\Lambda}{8\pi}, \qquad w' = \frac{P'}{\rho'}. \tag{2.27}$$

With this parametrization, (2.25) beautifully reduces to

$$\delta = \frac{1}{4}(1 + 3w'). \tag{2.28}$$

When the fermions are embedded in a uniform matter background, we expect the metric field solution of the ED system A to approach (2.22). At a large enough radius, the effects of the particles on the metric will become more and more negligible, and the numerical metric field solutions for A and T should tend to (2.23) and (2.24).

3. Einstein-Dirac solitons

3.1 Solving the Einstein-Dirac system numerically

In order to find the initial conditions necessary to solve the ED system of equations numerically, we follow the approach by FSY and assume that the fields behave regularly close to the origin. We compute the small r expansions of the metric and fermion fields for the ED system with a non-zero cosmological costant (see Appendix C). We find

$$\alpha(r) = \alpha_1 r^{N/2} + ... \tag{3.1}$$

$$\beta(r) = \frac{1}{N+1}(\omega T_0 - m)\alpha_1 r^{N/2+1} + ... \tag{3.2}$$

$$A(r) = 1 - \frac{\Lambda}{3}r^2 - 8\pi\omega T_0^2 \alpha_1^2 \frac{N}{N+1} r^N + ... \tag{3.3}$$

$$T(r) = T_0 + \sum_{k=1}^{N/2} \left(\frac{\Lambda}{3}\right)^k \frac{(2k-1)!!}{2k!!} T_0 r^{2k} - 4\pi T_0^2 \alpha_1^2 \frac{1}{N+1}(2T_0\omega - m) r^N + ... \tag{3.4}$$

where T_0, α_1, m, Λ and ω are free parameters. Note that we have chosen $\sigma = 1$ since we are interested in fermion dominated solutions with positive parity (instead of anti-fermion dominated ones with $\sigma = -1$). Using the above expansions, we initialize Mathematica's built in differential equation solver NDSolve at $r_i = 10^{-5}$.

In order to have physically sensible solutions, FSY impose two conditions: that the fermion fields are normalized

$$\int_0^\infty \frac{4\pi T}{\sqrt{A}}(\alpha^2 + \beta^2)dr = 1; \tag{3.5}$$

and that the metric is asimptotically Minkoswkian, i.e.,

$$\lim_{r\to\infty} A(r) = 1, \qquad \lim_{r\to\infty} T(r) = 1. \tag{3.6}$$

With a non-zero cosmological constant, (3.6) is not respected. Instead, we demand that A and T go over to the Scharzchild-(anti-)De Sitter metric at large r. Formally, that translates to

$$\lim_{r\to\infty} \sqrt{A(r)}T(r) = 1. \tag{3.7}$$

To impose (3.5) and (3.6), FSY solve the system of equations first, and then rescale the solutions. The rescalings enforce the above conditions to be respected. They define new weaker constraints

$$l = \sqrt{\int_0^\infty \frac{4\pi T_u}{\sqrt{A_u}}(\alpha_u^2 + \beta_u^2)dr} < \infty, \tag{3.8}$$

$$\tau = \lim_{r\to\infty} T_u(r) < \infty, \tag{3.9}$$

where the subscript u denotes the unscaled solutions. They also set $T_0 = 1, m = \pm 1$, where the positive/negative sign of m gives the fermion/antifermion solutions. To determine τ we use

$$\tau = \lim_{r\to\infty} \sqrt{A_u(r)}T_u(r). \tag{3.10}$$

The rescaled solutions are

$$\alpha(r) = \sqrt{\frac{\tau}{l}}\alpha_u(lr), \tag{3.11}$$

$$\beta(r) = \sqrt{\frac{\tau}{l}}\beta_u(lr), \tag{3.12}$$

$$A(r) = A_u(lr), \tag{3.13}$$

$$T(r) = \frac{1}{\tau}T_u(lr). \tag{3.14}$$

For the these to satisfy the ED equations, physical quantities need to be rescaled as well as follows

$$m = lm_u, \qquad \omega = l\tau\omega_u, \qquad \Lambda = l^2\Lambda_u. \tag{3.15}$$

At this point, the only parameters left to set are Λ, α_1 and ω. For $\Lambda = 0$, solutions exist for all choices of positive α_1. It is instructive to see how FSY results change when different values of Λ is included, so we set $\alpha_1 = 0.02$ and $N = 2$ as they did. We change Λ on a case by case basis to study whether solitonic solutions occur. We implement a binary search algorithm in ω which shoots for convergence of the fermion fields at large r. We then construct the unscaled solutions (see Appendix D), from which the scaled solutions can be obtained by following the procedure outlined above.

3.2 FSY solitons

To test the algorithm, we set $\Lambda = 0$ and reproduce the results by FSY, which are displayed in Fig. 3.1 below. The fermions self-organize in shell-like structures around the origin, where α dominates over its anti-fermion counterpart. At small r, α behaves linearly and β quadratically, as described by (3.1), (3.2). This is the "core" zone of the soliton. At larger r, we can qualitately explain the behaviour of α and β by disregarding the r^{-1} term in (2.8) and (2.9). Since A and T tend to 1, α looks like

$$\alpha'' \approx (m^2 - \omega^2 T^2)\alpha, \tag{3.16}$$

and similarly does β. Clearly, as long as $\omega T > m$, the system will display oscillatory behaviour: this is the wave zone. The ground state has no nodes, so we effectively observe no oscillations in Fig. 3.1. For $\omega T < m$, they system enters an evanescent zone characterized by exponential decay.

Much of the physics that makes ED solitons objects worth of study is summarised very well in Fig. 3.1. The Schwarzchild metric, which describes the structure of spacetime arising from a point mass in Einstenian gravity, diverges near the mass location.

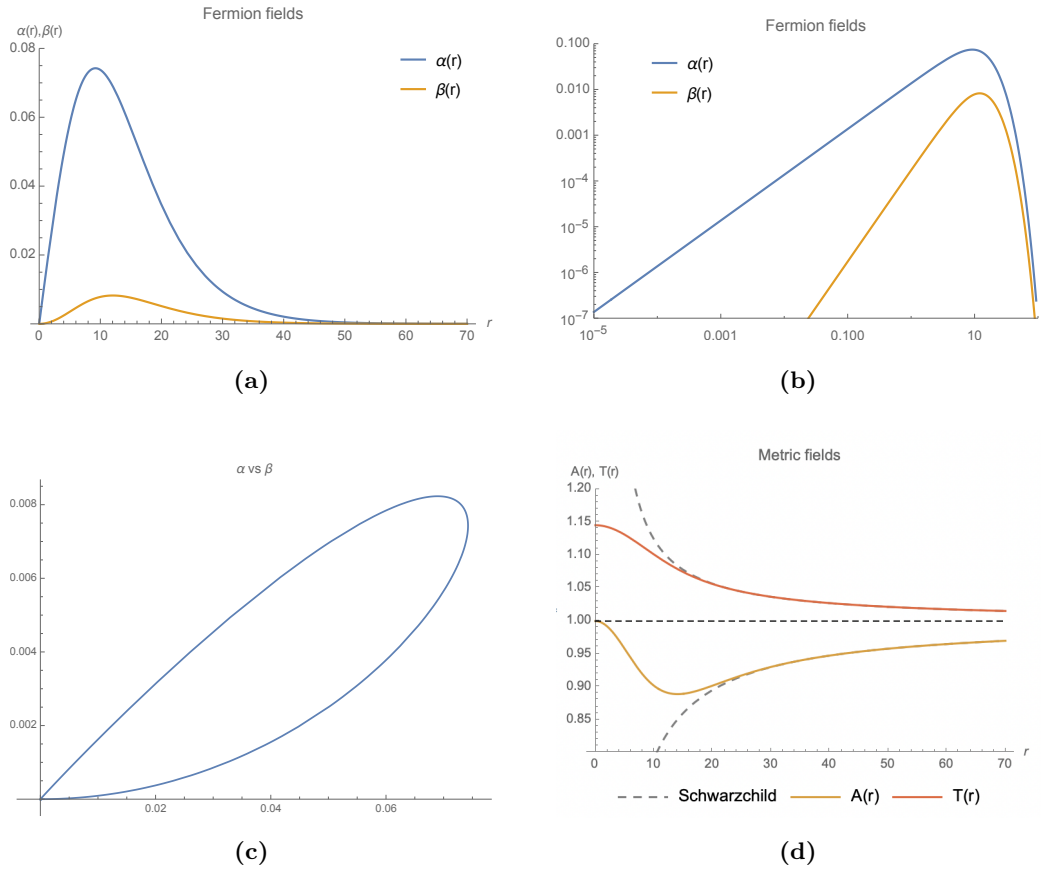

Figure 3.1: These graphs show the FSY ground state solutions to the ED equations. The fitted ADM mass from the Schwarzchild form of A and T is respectively $M = 1.0465$ and $M = 1.0461$, reasonably close to $M = 1.0467$ as calculated in [20]. The rescaled mass and frequency are $m = 0.5339$, $\omega = 0.4993$, very close to $m = 0.5340$, $\omega = 0.4994$ as calculated by FSY [15].

The metric fields A and T, however, are finite and well behaved at the origin. This happens because matter shrinking to a point is not consistent with quantum mechanics. Deeply hardwired

into the ED system (via the Dirac equation) is the Heisenberg uncertainty principle, which effectively "cures" the unphysical singularity at the origin. As a result, the fermions spread out in Planck-scale gravitationally localized structures, which take the name of ED solitons. At large r, as expected, the spacetime disturbance is indistinguishable from that of a point mass, and the Schwarzchild form is recovered.

3.3 Non-zero cosmological constant

In this section, we consider the ED system with non-zero cosmological constant. For positive Λ, we find solitonic solutions up to $\Lambda_u = 0.0001$, as shown in Fig. 3.2 below.

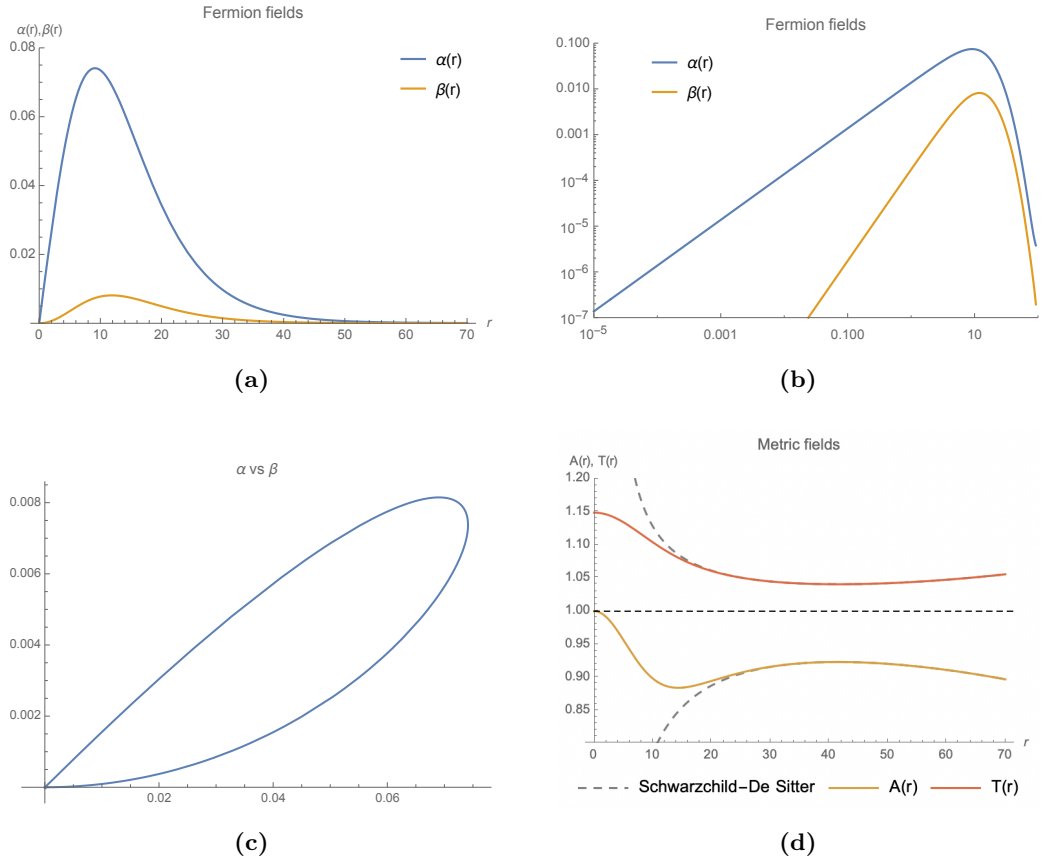

Figure 3.2: These graphs show the ground state solutions to the ED equations in the presence of $\Lambda_u = 0.0001$. The fitted ADM mass from the Schwarzchild form of A and T is respectively $M = 1.0623$ and $M = 1.0627$. The rescaled mass, frequency and cosmological constant are $m = 0.5438$, $\omega = 0.5065$, $\Lambda = 4.4 \cdot 10^{-5}$.

These results respect both (3.5) and (3.6): they are normalizable and the metric fields approach the Schwarzchild-De Sitter metric at large r, as displayed in Fig. 3.2. The curvature of the metric fields, since Λ is small, takes some time to kick in. The metric has a cosmological horizon at $r \sim 320$, where A crosses zero. The fermion fields retain their power law and exponential decaying behaviour respectively in the core and evanescent zones.

When Λ is negative, we find that EDS clearly occur for $-0.1 < \Lambda < 0$. For larger values, however, the behaviour of the fermion fields in the evanescent zone changes dramatically. An extreme case, $\Lambda_u = -10$, is displayed in Fig. 3.3 below.

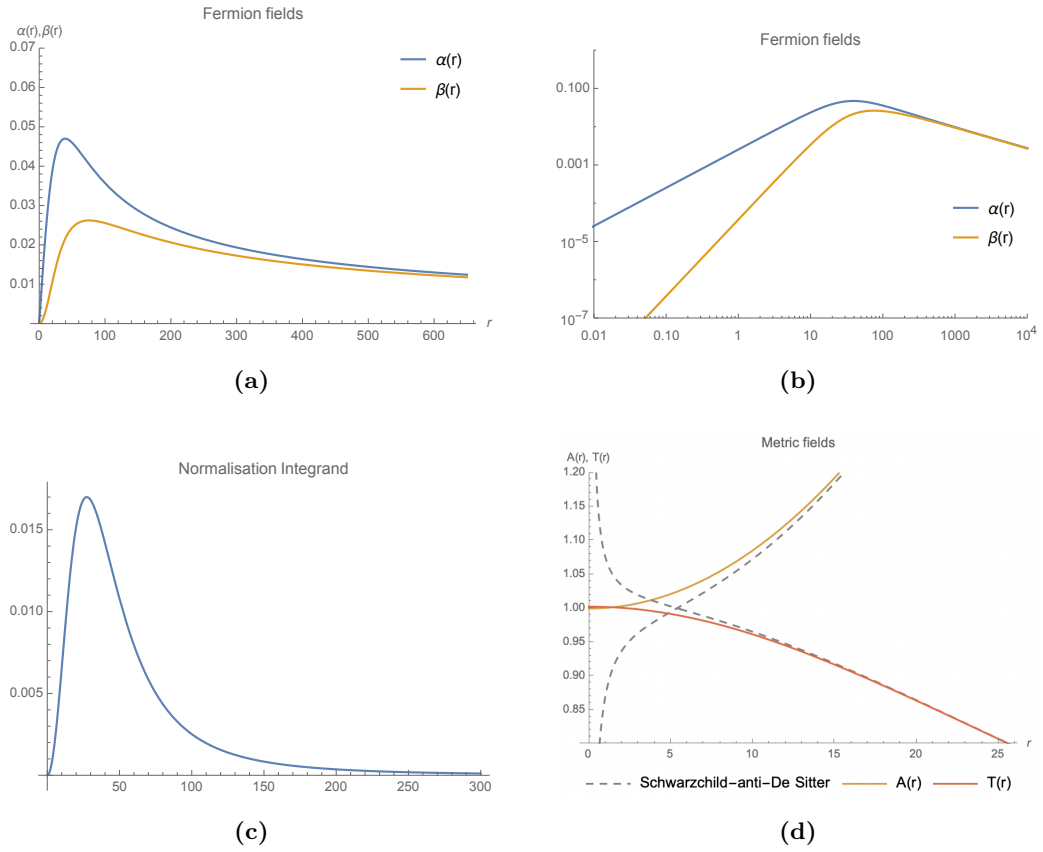

Figure 3.3: These graphs show the ground state solutions to the ED equations in the presence of $\Lambda_u = -10$. The extracted ADM mass from A is $M = 0.06677$ and from T is $M = 0.0699$. The rescaled mass, frequency and cosmological constant are $m = 0.0161$, $\omega = 0.06$ and $\Lambda = -0.0026$.

The metric fields approach the Schwarzchild-anti-De Sitter metric, as expected. α and β do not converge anymore, with tails extending to infinity. The power law of the core zone is

retained, but they display a power law decay at large r. Fitting the tails gives a decay that scales as $\sim r^{-1/2}$. Looking at the normalisation integral (3.5), the contribution from the metric fields is $1/r^2$, which means that convergence is achieved. This is similar to the behaviour of the conformal gravity-Dirac-Higgs solitons in [20].

For $\Lambda > 0.0001$, EDS do not occur. The fermion fields undergo oscillations of increasing frequency around 0, until they hit the cosmological event horizon, where NDSolve stops the evaluation. This behaviour is displayed in Fig. 3.4 below.

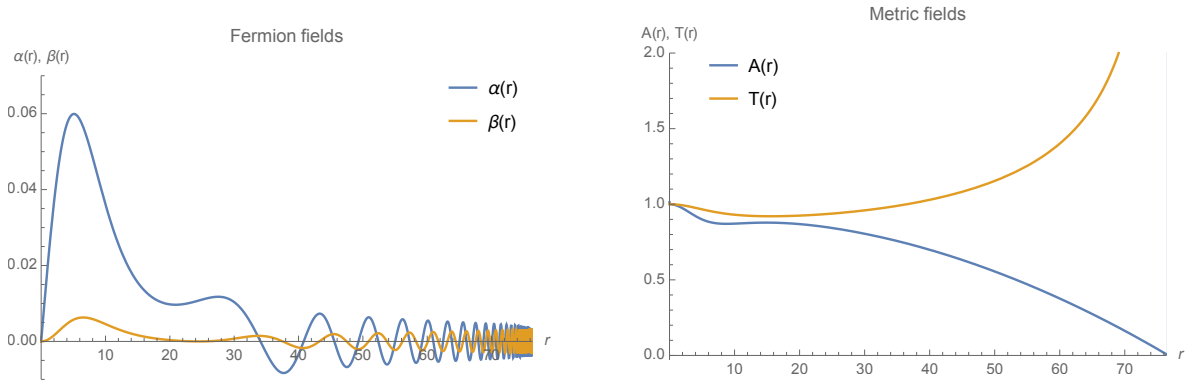

(a) **(b)**

Figure 3.4: These graphs show non-converging solutions to the ED equations in the presence of $\Lambda = 0.0005$. Where A vanishes lies the cosmological horizon, at $r = 76.67$.

We interpret this effect as a direct consequence of the proximity of the horizon to the location of the particles. This is supported by the observation that the amplitude of the oscillations increases with the value of Λ, which effectively corresponds to the cosmological horizon moving closer to the origin. For very small values of positive Λ, α and β converge at $l_p \sim 20$. On the other hand, for $\Lambda > 0.0001$, localization in the form of EDS does not occur. The particles are attracted by the gravitational pull of the horizon, into which they leak. The dynamics which enters the system due to this mechanism implies that a solution in this regime cannot exist, since it breaks the fundamental assumption that the system is time-independent on which the metric (2.3) is based.

For $\Lambda < 0$, A diverges at infinity. As Λ becomes more negative, the solutions start to get more spread out. We identify the origin of this phenomenon in the gravitational attraction from

the uniformly curved metric, which causes the fermion fields characteristic decay to slow down from an exponential one to a power law one. In other words, the particles are dragged away and get delocalized over all of space. However, since the infinity of the metric is very far away, the pull is very slow, so that the timescales of this process are much longer than the typical Planck timescales of EDS. In this way, the fundamental assumption about the time-independence of the system holds. These results suggest that a localization regime exists between two critical values of Λ, a positive and a negative one, in the middle of which EDS occur.

3.4 Uniform matter background

In this section, we consider a new version of the ED system which, on top of a non-zero cosmological constant, considers a matter background characterized by uniform density ρ and uniform isotropic pressure P. Einstein equations (2.10) and (2.11) respectively become

$$rA' = 1 - A - \Lambda r^2 - 8\pi(N\omega T^2(\alpha^2+\beta^2) + \rho), \tag{3.17}$$

$$2rA\frac{T'}{T} = A - 1 + \Lambda r^2 - 8\pi\left(N\omega T^2(\alpha^2+\beta^2) - \frac{N^2\sigma}{r}T\alpha\beta - 8\pi NmT(\alpha^2-\beta^2) + P\right), \tag{3.18}$$

while the Dirac equation components (2.8) and (2.9) remain the same. The small r expansions are given by (see Appendix C)

$$A(r) = 1 - \frac{1}{3}(\Lambda + 8\pi\rho)r^2 - 8\pi\omega T_0^2\alpha_1^2\frac{N}{N+1}r^N + ... \tag{3.19}$$

$$T(r) = T_0 + \sum_{k=1}^{N/2}\left(\frac{1}{3}\right)^k \frac{(\Lambda(2k-1) + 4\pi\rho(4k-5-3w))!!}{2k!!}T_0 r^{2k} - 4\pi T_0^2\alpha_1^2\frac{1}{N+1}(2T_0\omega - m)r^N + ... \tag{3.20}$$

Note that, by setting $\rho = 0$ and $P = 0$, one recovers (3.1)-(3.4). The pressure and energy density are rescaled as follows

$$\rho = l^2\rho_u, \qquad P = l^2 P_u. \tag{3.21}$$

We find EDS for a variety of combinations of Λ, ρ and P. In Fig. 4.4 below, we report the solutions for $\Lambda_u = 0$, $\rho = 1 \cdot 10^{-5}$ and $P = 3.3 \cdot 10^{-6}$. The effective equation of state for these parameters is $w' = 1/3$, which corresponds to a radiation background.

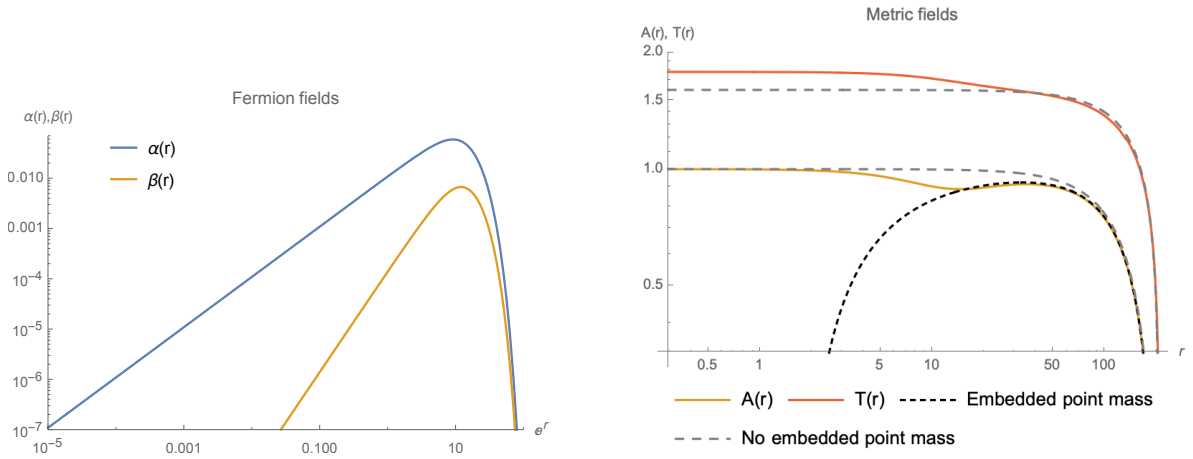

(a) **(b)**

Figure 3.5: These graphs show the ground state solutions to the ED equations in the presence of $\Lambda_u = 0$, $\rho_u = 1 \cdot 10^{-5}$, $P_u = 3.3 \cdot 10^{-6}$. The equation of state is $w' = 1/3$. In the right panel, the gray dashed lines are the analytical solutions for A and T in the presence of a uniform matter background and no embedded point mass: (2.23), (2.24). The black dashed line is the fitted analytical solution for A in presence of a uniform background and a point mass at the origin: (2.22). The extracted ADM mass is $M = 0.8361$. The rescaled physical quantities are $m = 0.5270$, $\omega = 0.3170$, $\rho = 2.7769 \cdot 10^{-6}$, $P = 9.2565 \cdot 10^{-7}$.

The fermion fields display power law behaviour at small r, in the core zone, as expected from the Taylor expansions, and decay exponentially in the evanescent zone. At large r, the metric field A approaches the solution to Einstein equations in the presence of a uniform matter background and embedded point mass (2.22) faster than it approaches the solution where no point mass is present (2.23). This is expected since (2.22) is a better description of the system, which is characterized by a finite ADM mass. As expected, T approaches (2.24).

4. A model for the formation of Einstein-Dirac solitons

4.1 Scope

In this section we introduce a model which can be used to investigate the formation of EDS for matter backgrounds characterized by different values of energy density and pressure. The matter background is reproduced by filling 3D space with clusters of fermions, all of which constitute an EDS. It is then possible to solve for a system at the origin which is influenced by the energy density and pressure of the surroundings, probing whether solitonic condensation occurs.

When the density is extremely low, the fermions are so far away that they do not influence each other. In this limit, the stress-energy tensor is effectively described by (2.7), so that the conditions for which we found EDS in Section 3.2 and Section 3.3 are recovered. However, as the density increases, α and β from different clusters overlap with each other, contributing to the energy density and pressure of the respective stress-energy tensors. In this regime, at low enough densities, we expect to recover the results of Section 3.4.

While the approach adopted in that section allowed to look at whether EDS form for specific values of the energy density and pressure, the model that we present here was designed to describe a time-dependent process. The density of the matter background is parametrized by the distance between the fermionic clusters, which can be identified as the scale factor of the Robertson-Walker metric. The Friedmann equations then describe an expansion driven by the background energy density and pressure. Note that, as before, provided that the process happens on timescales much larger than EDS timescales, the assumption that the metric (2.3) is time-independent is not broken. Thus, our model could form the basis to explore the analogy between particle formation in the early universe and the occurrence of solitonic structures.

4.2 Set-up

We model a uniform matter background by filling space with M spheres of radius R disposed in hexagonal close-packed (HCP) arrangement. Note that, since closest neighbouring balls are touching, the distance between their centres is $2R$. HCP achieves the closest packing possible of 3D space with identical 3-spheres, occupying 74% of the volume. It alternates two identical layers, as displayed below in Fig. 7.

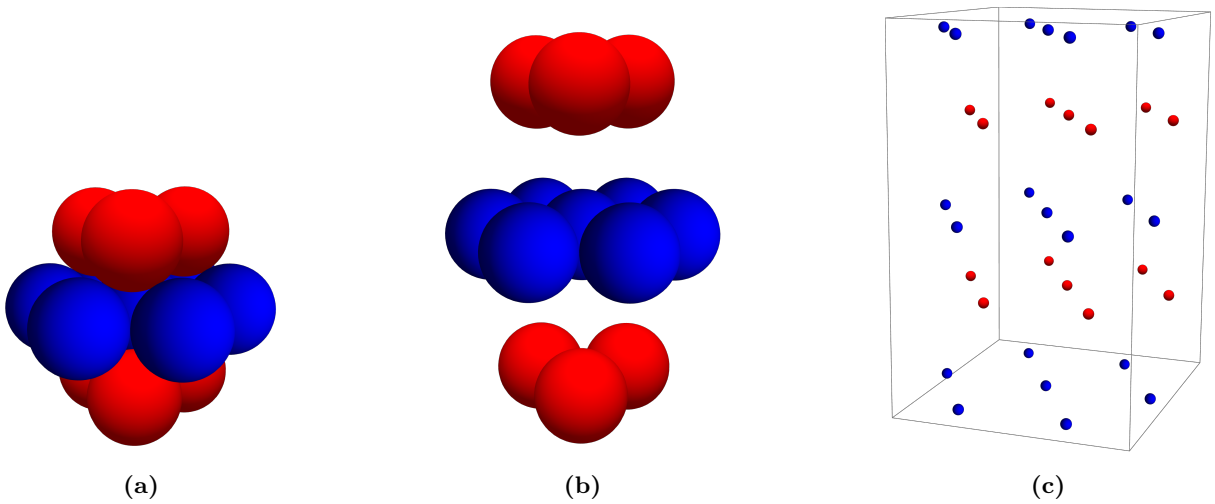

(a) **(b)** **(c)**

Figure 4.1: Balls in HCP arrangement. Each ball touches 12 surrounding balls, 6 in the equatorial plane, 3 above and 3 below. The alternation of the two identical layers generates a three-fold symmetry in the equatorial plane of each ball. For any 4 balls that all touch each other, their nuclei are the vertices of a regular tetrahedron of side $2R$. This arrangement is highly symmetric. Each ball can be regarded as the site of a lattice, where all the sites equivalent to each other.

At the nucleus of each sphere n lies a cluster of N fermions, the position of which we denote by $p_n = (x_n, y_n, z_n)$. We leave the ball at $p_0 = \{0, 0, 0\}$ empty as that is where we place the central system to be solved for. The fermionic number density is parametrized by R. We decide the number of balls to generate to fill space by setting R and r_{max}, where r_{max} denotes the maximum distance of a nucleus from the centre. For $2R > r_{max}$, space is empty, while for $2R = r_{max}$, we are only generating the 12 nearest neighbours to the central ball. Note that the shells composed by the nuclei of the neighbouring balls get closer to each other the farther away from the origin. For example, the distance of the shell composed by the nuclei of the 2^{nd} nearest

neighbours is less than $4R$. Infinitely far away, the shells merge into a continuum.

We model each cluster by centering a copy of our solitonic solutions at p_n. We denote the scaled fields that compose these solutions $\bar{\alpha}, \bar{\beta}, \bar{A}, \bar{T}$. Thus, the n^{th} soliton at p_n is described by $\bar{\alpha}_n, \bar{\beta}_n, \bar{A}_n, \bar{T}_n$, where

$$\bar{\alpha}_n = \bar{\alpha}(x - x_n, y - y_n, z - z_n), \tag{4.1}$$

and the other fields are similarly defined.

We calculate the effect of this packing on spacetime by determining the cumulative energy density and pressure from all the clusters. These are the components of the stress-energy tensor (2.7), which can be expressed more succinctly as

$$T^{\mu}_{\nu} = diag(\rho, P_r, P_\phi, P_\theta) = diag\left(\frac{N\omega T^2}{r^2}(\alpha^2 + \beta^2), \frac{N\,T\,\sqrt{A}}{r^2}(\alpha\,\beta' - \beta\,\alpha'), \frac{N\sigma\,T\,\alpha\,\beta}{2\,r^3}, \frac{N\sigma\,T\,\alpha\,\beta}{2\,r^3}\right).$$

The behaviour of the energy density and radial pressure of individual EDS originated from different values of Λ is shown is Fig. 4.2 below. The azimuthal and polar pressures behave similarly. Note that EDS get more spread out as Λ departs from zero, which reflects the findings of Section 3.3.

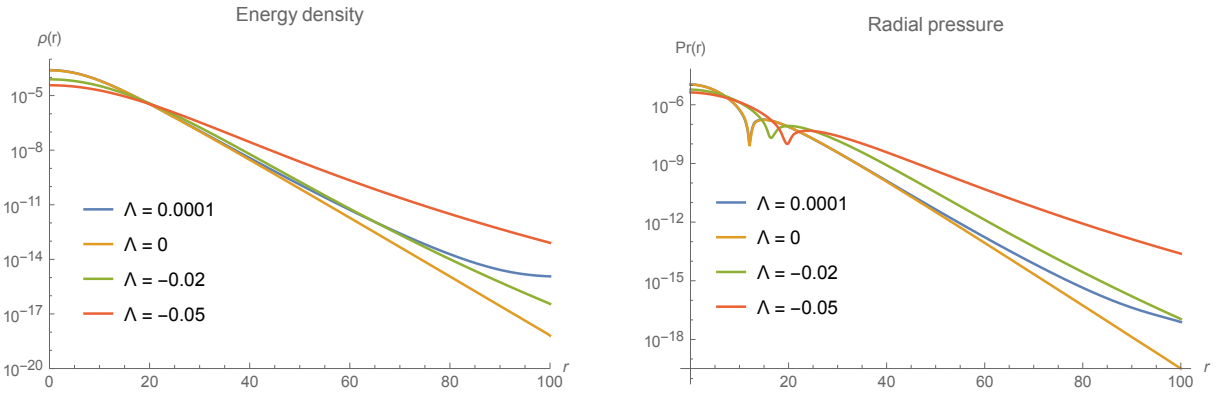

(a) **(b)**

Figure 4.2: The graphs show the energy density and radial pressure of individual EDS that originated from different $\Lambda = -0.05$, $\Lambda = -0.02$, $\Lambda = 0$ and $\Lambda = 0.0001$. In the left panel, the absolute value of the radial pressure is plotted. The pressure crosses zero where the spike occurs in the curves, to then approach zero from below.

We write the cumulative energy density and pressures from a coordinate system that is

centred at the origin. This coordinate system should be in spherical coordinates, since our ED equations are defined in a spherically symmetric scenario where all fields are functions of radius only. The energy density is a scalar quantity, so determining its cumulative value ρ_{tot} at each point is straightforward:

$$\bar{\rho}_{tot}(x,y,z) = \sum_{n=1}^{M} \bar{\rho}_n, \tag{4.2}$$

where

$$\bar{\rho}_n(x,y,z) = \frac{N\bar{\omega}\bar{T}_n^2}{r^2}(\bar{\alpha}_n^2 + \bar{\beta}_n^2). \tag{4.3}$$

We aim to have a function of the energy density that depends only on radius. We calculate the average of ρ_{tot} over the solid angle 4π for a range of radii $0 \leq r_v \leq r_{max} + \epsilon$ and interpolate the results. Farther than r_{max} space is empty, so we usually choose ϵ to be the distance at which the EDS energy density and pressures go to an infinitesimal value. Note that EDS from larger values of Λ decay more slowly and will need larger ϵ. We calculate the average of ρ_{tot} over a sphere of radius r_v by implementing the Monte-Carlo method

$$\rho_{avg}(r_v) = \frac{1}{N}\sum_{i}^{N} \bar{\rho}_{tot}(r_v, \phi_i, \theta_i), \tag{4.4}$$

for $0 \leq \phi_i \leq 2\pi$, $0 \leq \theta_i \leq \pi$. As low as 400 points is usually enough to a achieve sensible results, with a relative uncertainty of order 0.01. An interpolation of the values computed for ρ_{avg} at all the radii finally yields the spherically symmetric background energy density $\rho_s(r)$, where by the subscript s we denote that it originates from the surrounding balls.

Taking into account the pressures is more complicated. Depending on the location in space, the pressures from each ball contribute in different amounts to the pressures that are seen by the central system. Ball n is characterised, in its coordinate frame, by some $\bar{P}_r, \bar{P}_\phi, \bar{P}_\theta$. The magnitude of these is

$$\bar{P}_{r_n}(x,y,z) = \frac{N\bar{T}_n\sqrt{\bar{A}_n}}{r^2}(\bar{\alpha}_n\bar{\beta}_n' - \bar{\beta}_n\bar{\alpha}_n'), \tag{4.5}$$

$$\bar{P}_{\phi_n}(x,y,z) = \bar{P}_{\theta_n}(x,y,z) = \frac{N\sigma\bar{T}_n\bar{\alpha}_n\bar{\beta}_n}{2r^3}. \tag{4.6}$$

At each point in space, each one of these pressures points in different directions. We would like to obtain, at large r where the number of balls taken into account is very high, an isotropic uniform pressure. Isotropic uniform pressure and energy density are fundamental conditions that the model needs to reproduce. Without them, further developments to link it to the Friedmann equations, which are built on the assumption of a perfect fluid, would not be possible.

Computing the pressures from balls at fixed points would be a source of anisotropy. While averaging over the solid angle mimics an oscillation of the balls in the θ and ϕ directions, the fact that they are fixed at a particular radial distance would still contribute to variations in the values of the three pressures at different radii. To impose pressure isotropy, we average the components from the surrounding balls as follows

$$\bar{P}_{tot}(x, y, z) = \sum_{n=1}^{M} \frac{1}{3}(\bar{P}_{r_n} + 2\bar{P}_{\phi_n}). \tag{4.7}$$

We then obtain $P_s(r)$ via Monte-Carlo and interpolation of the results, as we did for the energy density ρ_s.

4.3 Results

We expect the uniformity of ρ_s and P_s to improve with the number of balls that are computed for, since the shells of higher order neighbours get closer and closer together. This is displayed in Fig. 4.3 below. As the number of balls increases, the amplitude of the oscillations (i.e., the strength of the variations of either the pressure or the energy density from an asymptotic value) keeps decreasing. This shows that the background uniformity necessary to reproduce perfect fluid conditions is achieved.

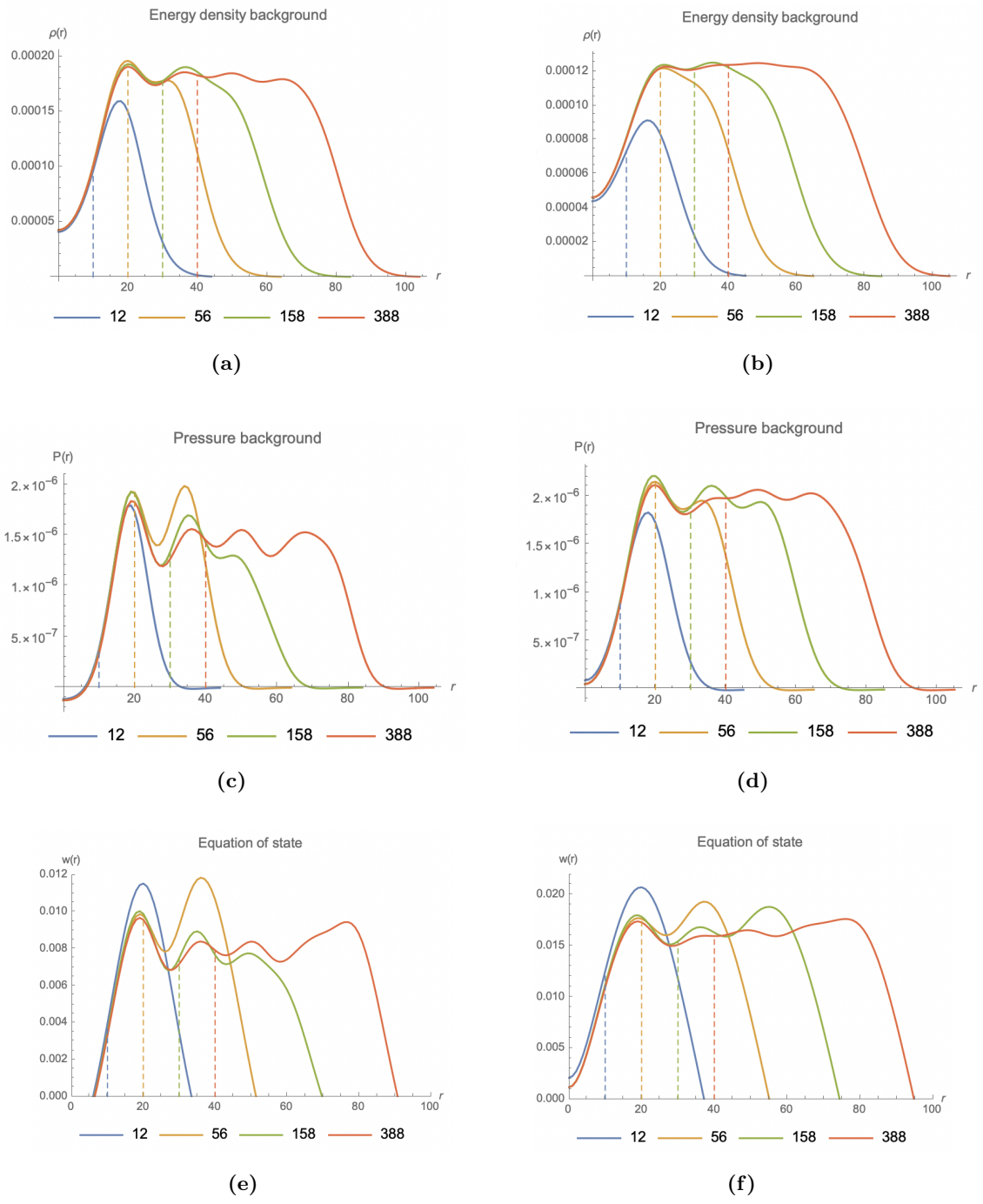

Figure 4.3: These graphs show the pressure, energy density and equation of state generated by 12, 56, 158 and 388 balls of $R = 10$. The values of r_{max} are respectively 20, 40, 60 and 80. The dashed colored lines mark the point $r_{max}/2$ for the different curves, namely the point at which the background starts to feel the vacuum of $r > r_{max}$. The left and right columns shows graphs for balls at which nuclei lie EDS from $\Lambda = 0$ and $\Lambda = -0.01$ respectively.

Now that we have a model for the background matter, we proceed to solve for N fermions at the origin. We update the stress energy tensor by adding the pressure and energy density of the surrounding balls. We can do so without breaking the spherical symmetry of the ED system since ρ_s and P_s are only functions of r. While the Dirac equation remain the same, the Einstein equations now are

$$rA' = 1 - A - \Lambda r^2 - 8\pi(\rho + \rho_s), \tag{4.8}$$

$$2rA\frac{T'}{T} = A - 1 + \Lambda r^2 - 8\pi(P_r + P_s). \tag{4.9}$$

We solve for the central system in the presence of the 12 nearest neighbours; the balls have radius $R = 20$. The result is reported in Fig. 4.4 below.

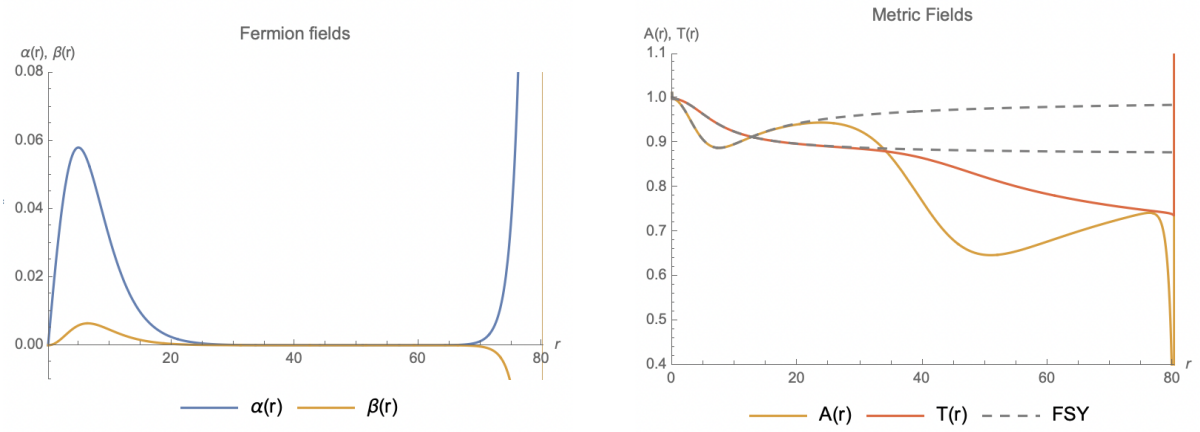

(a) **(b)**

Figure 4.4: These graphs show the unscaled solutions for a couple of fermions at the origin. The background is composed by 12 balls of R=20, sitting at a distance $d = 2R = 40$ from the origin. The cosmological constant $\Lambda = 0$. The EDS at the neighbouring nuclei are FSY ground state solitons. The dashed lines on the right panel are the metric fields of FSY EDS. At $r = 80.27$ the numerical solver stops evaluating.

The metric starts to respond to the background of the neighbouring balls at $r \sim 20$, where it deviates from the empty space FSY solution (see Fig. 3.1). After the perturbation, it slowly starts to recover its asymptotic behaviour in flat space, as expected.

Finite precision of the numerical solver NDSolve causes the fields to diverge at $r = 80.27$.

We suspect that this happens due to computational limitations that prevent the attainment of the required precision. We have attempted various Mathematica's built-in methods to force the solver to compute past the stiff point, such as StiffnessSwitching, Extrapolation, ExplicitRungeKutta and LSODA, although unsuccessfully. This prevented the construction of the scaled physical solutions.

If convergence of the fields were achieved, the next step would have been to copy and paste the new solitonic solution at the centre of all the neighbouring balls. The whole process detailed in the previous section (Section 4.2) would have then been repeated, thus re-updating the stress-energy tensor and re-solving for a system in the centre. This cycle would have been iterated until an eventual stabilisation of the solutions occurred (i.e., when updating the neighbours and re-solving for the centre stopped affecting the shape of the EDS forming at the origin). The system is inherently highly symmetric and, for large numbers of surrounding balls, characterized by a uniform and isotropic background. For this reason, the stabilisation of the solutions would have reflected a universe where fermions have condensed out in the form of EDS. Investigating different energy density regimes would have then been possible by simply varying the radius of the balls. If a phase transition for EDS formation exists, they would cease to occur for radii smaller than some critical value.

5. Summary & outlook

In this report, we have shown that EDS occur as solutions to a modified ED system that takes into account a non-zero cosmological constant and a uniform matter background. We have qualitatively identified a localisation regime for EDS bounded above and below by the cosmological constant, and we have proposed a physical interpretation of this behaviour that recognizes the cause of delocalization in the gravitational pull of the metric. Next, we have presented a model that might be used to investigate the behaviour and formation of EDS. The model utilizes EDS to reproduce an uniform matter background and is designed to solve for a system of fermions embedded in it. Computational limitations of the numerical solver terminate

the solutions at a finite small radius, preventing further study of EDS formation to be achieved at present.

The most natural development of this work would involve devising a way to improve the numerical technique to achieve convergence of the fields at large r when nearest neighbours are taken into account. The uniform matter background that the model reproduces forms the perfect basis to incorporate the Friedmann-Robertson-Walker metric and the Friedmann equations. This would allow to simulate an expanding universe where the energy density of the environment is rapidly decreasing, and to study EDS formation in this scenario. Finally, it would be interesting to investigate whether solitonic solutions occur when the electromagnetic and Higgs fields (Einstein-Dirac-Maxwell-Higgs system) are considered alongside a non-zero cosmological constant and a uniform matter background.

Bibliography

[1] A. Einstein. Erklärung der perihelbewegung des merkur aus der allgemeinen relativitätstheori. Königlich Preußische Akademieder Wissenschaften, 831–839 (1915). English version: Einstein's Paper:"Explanation of the Perihelion Motion of Mercury from General Relativity Theory". A. A. Vankov. General Science Journal, (2013).

[2] R. F. Carswell, D. Walsh, and R. J. Weymann. 0957+ 561 a, b: twin quasistellar objects or gravitational lens? Nature **279**, 381 (1979).

[3] B. P. Abbott et al. Observation of gravitational waves from a binary black hole merger. Physical review letters **116**, 061102 (2016).

[4] J. M. Butterworth. The standard model: how far can it go and how can we tell? Philosophical Transactions of the Royal Society A: Mathematical, Physical and Engineering Sciences **374**, 20150260 (2016).

[5] K. Krasnov and R. Percacci. Gravity and unification: A review. Classical and Quantum Gravity **35**, 143001 (2018).

[6] K. A. Meissner. Black-hole entropy in loop quantum gravity. Classical and Quantum Gravity **21**, 5245 (2004).

[7] L. Modesto. Loop quantum black hole. Classical and Quantum Gravity **23**, 5587 (2006).

[8] J. Brunnemann and T. Thiemann. On (cosmological) singularity avoidance in loop quantum gravity. Classical and Quantum Gravity **23**, 1395 (2006).

[9] V. Husain and O. Winkler. Quantum resolution of black hole singularities. Classical and Quantum Gravity **22**, L127 (2005).

[10] F. Kenneth and J. A. Wheeler. *Geons, black holes and quantum foam: a life in physics.* (American Association of Physics Teachers, 2000).

[11] I. Agullo, A. Ashtekar, and W. Nelson. Quantum gravity extension of the inflationary scenario. Physical review letters **109**, 251301 (2012).

[12] D. H. Coule. Quantum cosmological models. Classical and Quantum Gravity **22**, R125 (2005).

[13] D. R. Brill and J. A. Wheeler. Interaction of neutrinos and gravitational fields. Reviews of Modern Physics **29**, 465 (1957).

[14] T. D. Lee, Y. Pang. Fermion soliton stars and black holes. Physical Review D **35**, 3678 (1987).

[15] F. Finster, J. Smoller, and S. T. Yau. Particle-like solutions of the Einstein-Dirac equations. Physical Review D **59**, 104020 (1999).

[16] N. S. Manton and P. Sutcliffe. *Topological solitons.* (Cambridge University Press, 2004).

[17] P. G. Drazin and R. S. Johnson. *Solitons: an introduction.* (Cambridge university press, 1989).

[18] F. Finster, J. Smoller, and S. T. Yau. Particle-like solutions of the Einstein-Dirac-Maxwell equations. Physical Letters A **259**, 431-436 (1999).

[19] F. Finster, J. Smoller, and S. T. Yau. The interaction of Dirac particles with non-abelian gauge fields and gravity-bound states. Nuclear Physics B **584**, 387-414 (2000).

[20] A. D. Leggat. Dirac solitons in general relativity and conformal gravity. PhD Thesis, University of St Andrews (2017).

[21] D. G. Dritschel, C. A. Hooley, K. Horne, and P. E. D. Leith. Fermion self-trapping in the optical geometry of Einstein-Dirac solitons. Physical Review D **101**, 106012 (2020).

[22] D. B. Canário, C. A. Hooley, K. Horne, and S. Lloyd. Infinite-redshift localized states of dirac fermions under einsteinian gravity. Physical Review D **102**, 084049 (2020).

[23] C. H. R. Herdeiro, A. M. Pombo, and E. Radu. Asymptotically flat scalar, Dirac and Proca stars: discrete vs. continuous families of solutions. Physical Review B **773**, 654-662 (2017).

[24] C. Herdeiro, I. Perapechka, E. Radu, and Y. Shnir. Asymptotically flat spinning scalar, Dirac and Proca stars. Physical Review B **797**, 134845 (2019).

[25] F. Finster, J. Smoller, and S. T. Yau. Non-existence of time-periodic solutions of the Dirac equation in a reissner-nordström black hole background. Journal of Mathematical Physics **41**, 2173-2194 (2000).

[26] F. Finster, J. Smoller, and S. T. Yau. Non-existence of black hole solutions for a spherically symmetric, static Einstein-Dirac-Maxwell system. Communications in mathematical physics **205**, 249-262 (1999).

[27] Y. Bernard. Non-existence of black-hole solutions for the electroweak Einstein-Dirac-Mang mills equations. Classical and Quantum Gravity **23**, 4433 (2006).

[28] J. Rafelski and J. Birrell. Traveling through the universe: Back in time to the quark-gluon plasma era. Journal of Physics: Conference Series **509**, 012014 (2014).

[29] J. Podolsky. The structure of the extreme schwarzschild-de sitter space-time. General Relativity and Gravitation **31**, 1703–1725 (1999).

[30] D. Tong. Lectures on general relativity. University of Cambridge, Department of Applied Mathematics and Theoretical Physics (2019).

[31] R. A. d'Inverno. *Introducing Einstein's relativity.* (Clarendon Press, 1992).

[32] R. S. Irving. *Integers, polynomials, and rings: a course in algebra.* (Springer Science & Business Media, 2003).

Appendix A.

Solution to (2.14) via the integrating factor method

We rewrite (2.14) in standard form

$$\frac{dT}{dr} + T\left(-\frac{1}{2r} + \frac{1}{2rA} - \frac{\Lambda r}{2A}\right) = \frac{dT}{dr} + Ta(r) = 0. \tag{A.1}$$

We proceed by multiplying both sides by the integrating factor and contracting into the derivative of a product

$$\exp\left(\int a(r)dr\right)\frac{dT}{dr} + Ta(r) = \frac{d}{dr}\left(T\exp\left(\int a(r)dr\right)\right) = 0. \tag{A.2}$$

Integrating both sides and rearranging for T we find

$$T(r) = \frac{C}{\exp\left(\int a(r)dr\right)}, \tag{A.3}$$

where C is an integration constant. Substituting (2.15) into $a(r)$ and rearranging gives the integral

$$\int a(r)dr = -\int \frac{dr}{2r} + 3\int \frac{(1-\Lambda r^2)dr}{6r + 6c_1 - 2\Lambda r^3}, \tag{A.4}$$

which can be solved with the substitution $u = 6r + 6c_1 - 2\Lambda r^3$. The result is

$$\int a(r)dr = \ln\left(\sqrt{6 + \frac{6c_1}{r} - 2\Lambda r^2}\right) + D, \tag{A.5}$$

where D is an integration constant. Rearranging and subbing into (A.3) finally gives

$$T(r) = \frac{c_2}{\sqrt{1 + c_1/r - \Lambda r^2/3}}, \tag{A.6}$$

where $c_2 = C\exp(-D)/\sqrt{6}$.

Solution to (2.21) via the integrating factor method

To solve (2.21) for the case of $M = 0$, we adopt the same procedure that we used to solve (2.14). The relevant integrating factor is

$$a(r) = -\frac{1}{2r} + \frac{1}{2rA} - \frac{8\pi P' r}{2A}, \tag{A.7}$$

where

$$A(r) = 1 - \frac{8\pi}{3}\rho' r^2. \tag{A.8}$$

Rearranging yields

$$\int a(r)dr = \frac{4\pi}{3}\int \frac{(\rho' + 3P')rdr}{1 - 8\pi/3\rho' r^2}, \tag{A.9}$$

which can be solved with the substitution $u = 1 - 1/3(\Lambda + 8\pi\rho)r^2$. The result is

$$\int a(r)dr = -\delta \ln\left(1 - \frac{1}{3}(\Lambda + 8\pi\rho)r^2\right) + F, \tag{A.10}$$

where

$$\delta = \frac{8\pi(\rho + 3P) - 2\Lambda}{4(\Lambda + 8\pi\rho)}, \tag{A.11}$$

and F is an integration constant. So we have that

$$T(r) = \frac{G}{\exp(-\delta \ln(A) + F)}, \tag{A.12}$$

where G is the integration constant from the integration step analogous to (A.2). We rearrange to get

$$T(r) = c_3 A^{\delta}, \tag{A.13}$$

where $c_3 = G\exp(-F)$.

Appendix B.

Determination of the roots of A

We want to find the roots of the metric field A

$$A(r) = \frac{1}{r}\left(r + -2M - \frac{\Lambda r^3}{3}\right). \tag{B.1}$$

A general cubic equation

$$ax^3 + bx^2 + cx + d = 0 \tag{B.2}$$

has discriminant

$$\Delta = 18abcd - 4b^3d - 4ac^3 - 27a^2d^2. \tag{B.3}$$

We consider real coefficients, since M and Λ are physical values. There are three cases: if $\Delta > 0$, then there are three distinct real roots; if $\Delta < 0$, then there is one real root and two complex roots that are the complex conjugates of each other; if $\Delta = 0$, then all of the roots are real and at least two roots coincide [32]. The discriminant of A is

$$\Delta = \frac{4}{3}\Lambda(1 - 9\Lambda M^2). \tag{B.4}$$

For $0 < \Lambda < 1/(9M^2)$, $\Delta > 0$ and A has three distinct real roots. For $\Lambda > 1/9M^2$ and $\Lambda < 0$, there is only one real root. We proceed to analyse the behaviour of (B.1) to locate the roots and the associated horizons.

For $\Lambda < 0$, the $-2M/r$ term dominates at small positive r, where it drives the metric to $-\infty$. As r gets larger, the cosmological quadratic term starts to dominate, causing A to diverge

to $+\infty$. Thus, for $\Lambda < 0$ the metric has one single horizon linked to the ADM mass term: this is the Schwarzchild black hole horizon.

For $\Lambda > 1/(9M^2)$, for $r < 0$ the metric is diverges to $+\infty$ close to zero, and decays to $-\infty$ at large r. This locates the only real root at negative r, which is not physical.

For $0 < \Lambda < 1/(9M^2)$, the $-2M/r$ term dominates at small r, which means that there is the Schwarzchild horizon. For $r < 0$, the $-2M/r$ term shoots to ∞ close to the origin. All the terms in the equation are positive a part from the cosmological one, which dominates at large negative r, and drives the system to $-\infty$. This implies that only one real root can be on the negative axis. The third real root must be on the positive axis at some radius larger than the Schwarzchild radius, where the cosmological term dominates. This is a cosmological horizon.

If $\Delta = 0$ then $\Lambda = 1/(9M^2)$. This is an extreme case where the cosmological and black hole horizons coincide [29].

Appendix C.

Small r expansion for ED equations with non-zero cosmological constant

The ED equations in presence of a non-zero Λ are

$$\sqrt{A}\alpha' = \frac{\sigma N}{2r}\alpha - (\omega T + m)\beta, \tag{C.1}$$

$$\sqrt{A}\beta' = -\frac{\sigma N}{2r}\beta + (\omega T - m)\alpha, \tag{C.2}$$

$$rA' = 1 - A - \Lambda r^2 - 8\pi N\omega T^2(\alpha^2 + \beta^2), \tag{C.3}$$

$$2rA\frac{T'}{T} = A - 1 + \Lambda r^2 - 8\pi N\omega T^2(\alpha^2 + \beta^2) + \frac{8\pi N^2\sigma}{r}T\alpha\beta + 8\pi N m T(\alpha^2 - \beta^2). \tag{C.4}$$

To calculate small r expansions for α, β, A, T, we use the following:

$$\alpha(r) = r^P(\alpha_1 + \alpha_2 r + \alpha_3 r^2 + ...) \tag{C.5}$$

$$\beta(r) = r^P(\beta_1 + \beta_2 r + \beta_3 r^2 + ...) \tag{C.6}$$

$$A(r) = A_0 + A_1 r + A_2 r^2 + ... + A_N r^N + ... \tag{C.7}$$

$$T(r) = T_0 + T_1 r + T_2 r^2 + ... + T_N r^N + ... \tag{C.8}$$

We substitute (C.5) - (C.6) into (C.3) - (C.4) and solve order by order to determine algebraic constraints for the coefficients.

At order r^0, (C.3) and (C.4) both give

$$A_0 - 1 = 0, \tag{C.9}$$

from which it follows that $A_0 = 1$.

At order r^{P-1}, (C.1) and (C.2) respectively give

$$P\alpha_1 r^{P-1} = \frac{\sigma N}{2r}\alpha_1 r^P, \tag{C.10}$$

$$P\beta_1 r^{P-1} = -\frac{\sigma N}{2r}\beta_1 r^P. \tag{C.11}$$

To satisfy these equations, we demand either $\sigma = 1, \beta_1 = 0$ and α_1 unconstrained; or $\sigma = -1, \alpha_1 = 0$ and β_1 unconstrained. The former gives the solution with positive mass, where the fermion field α is dominant, while the latter gives the antifermion one with negative mass, where β dominates. In both cases we have $P = N/2$. Note that we need $P > 0$ since we are performing a small-r expansion; r^P with $P < 0$ would diverge for small r. We choose the fermion branch.

At order r^{N-1}, (C.4) becomes

$$0 = 8\pi\frac{N^2}{r}T_0\alpha_1 r^{N/2}\beta_1 r^{N/2}, \tag{C.12}$$

which is satisfied by $\beta_1 = 0$ and leaves T_0 unconstrained.

At order r, (C.3) and (C.4) give respectively

$$rA_1 = -A_1 r, \tag{C.13}$$

$$2rT_1 = A_1 r T_0, \tag{C.14}$$

which imply $A_1 = 0, T_1 = 0$.

At order r^2, (C.3) and (C.4) give respectively

$$2A_2r^2 = -A_2r^2 - \Lambda r^2, \tag{C.15}$$

$$2r(1+...)(2T_2r+...) = (A_2r^2 + \Lambda r^2)(T_0+...). \tag{C.16}$$

(C.15) implies $A_2 = -\Lambda/3$, while (C.16) becomes

$$4T_2r^2 = \frac{2}{3}\Lambda T_0 r^2, \tag{C.17}$$

which gives $T_2 = 1/6\Lambda T_0$.

At order r^3, (C.3) gives

$$3A_3r^3 = -A_3r^3, \tag{C.18}$$

which implies $A_3 = 0$. We can see that $A_4, A_5, ..., A_{N-1}$ will similarly be zero.

For higher orders, (C.4) gives

$$2r\left(1-\frac{\Lambda}{3}r^2\right)\left(\frac{\Lambda T_0}{3}r + 3T_3r^2 + 4T_4r^3 + ...\right) = \left(\frac{2}{3}\Lambda r^2\right)\left(T_0 + \frac{\Lambda T_0}{6}r^2 + T_3r^3 + T_4r^4 + ...\right). \tag{C.19}$$

For r^3, this gives

$$6T_3r^3 = 0, \tag{C.20}$$

hence $T_3 = 0$. This is due to the fact that $T_1 = 0$. Similarly, all T_n with odd n up to T_{N-1} will be zero.

For r^4, (C.19) yields

$$2r\left(4T_4r^3 - \frac{\Lambda^2 T_0}{9}r^3\right) = \frac{2}{18}\Lambda^2 T_0 r^4, \tag{C.21}$$

which implies $T_4 = 1/24T_0\Lambda^2$. A similar calculation gives $T_6 = 5/432T_0\Lambda^3$.

We calculate the recursive relation between T_n and T_{n-2} for $2 \leq n \leq N-2$. We expand

(C.19) up to order $N-2$

$$2r\left(1-\frac{\Lambda}{3}r^2\right)\left(...+(N-4)T_{N-4}r^{N-5}+(N-2)T_{N-2}r^{N-3}\right)= \\ \frac{2}{3}\Lambda r^2\left(...+T_{N-4}r^{N-4}+T_{N-2}r^{N-2}\right). \quad \text{(C.22)}$$

We define $p=N-2$. N is an arbitrary even number, which means p is arbitrary as well. For r^p, we have

$$2r\left(pT_pr^{p-1}-\frac{\Lambda}{3}r^2T_{p-2}(p-2)r^{p-3}\right)=\frac{2}{3}\Lambda r^2T_{p-2}r^{p-2}, \quad \text{(C.23)}$$

from which we find, switching back to the usual index n,

$$T_n=\frac{\Lambda}{3}\frac{n-1}{n}T_{n-2}, \quad \text{(C.24)}$$

for $2\leq n\leq N-2$.

We therefore conclude

$$T_n=\left(\frac{\Lambda}{3}\right)^{n/2}\frac{(n-1)!!}{n!!}T_0, \quad \text{(C.25)}$$

which holds for $0\leq n\leq N-2$.

At order $r^{N/2}$, (C.1) and (C.2) give respectively

$$\alpha_2\left(\frac{N}{2}+1\right)r^{N/2}=\frac{N}{2r}\alpha_2r^{N/2+1} \quad \text{(C.26)}$$

$$\beta_2\left(\frac{N}{2}+1\right)r^{N/2}=-\frac{N}{2r}\beta_2r^{N/2+1}+(\omega T_0-m)\alpha_1r^{N/2}. \quad \text{(C.27)}$$

Equation (C.22) implies $\alpha_2=0$, while (C.23) implies

$$\beta_2=\frac{(\omega T_0-m)\alpha_1}{N+1}. \quad \text{(C.28)}$$

Higher order terms $\alpha_3,\beta_3,...$ are negligible at small r.

At order r^N, (C.3) gives while (C.4) gives

$$rNA_N r^{N-1} = -A_N r^N - 8\pi N\omega T_0^2 \alpha_1^2 r^N, \tag{C.29}$$

$$2r\left(T_N N r^{N-1} - \frac{\Lambda}{3}(N-2)T_{N-2}r^{N-1}\right) = \frac{2}{3}\Lambda T_{N-2}r^N + T_0 A_N r^N - 8\pi\left(N\omega T_0^2\alpha_1^2 r^N - \frac{N^2}{r}T_0\alpha_1\beta_2 r^{N+1} - NmT_0\alpha_1^2 r^N\right)T_0, \tag{C.30}$$

which yield

$$A_N = -\frac{8\pi N\omega T_0^2\alpha_1^2}{N+1} \tag{C.31}$$

$$T_N = \frac{\Lambda}{3}\frac{N-1}{N}T_{N-2} - \frac{4\pi T_0^2\alpha_1^2}{N+1}(2T_0\omega - m). \tag{C.32}$$

Using (C.23) to substitute for T_{N-2} gives

$$T_N = \left(\frac{\Lambda}{3}\right)^{N/2}\frac{(N-1)!!}{N!!}T_0 - \frac{4\pi T_0^2\alpha_1^2}{N+1}(2T_0\omega - m). \tag{C.33}$$

Having calculated all the necessary coefficients, we can rewrite (C.5) - (C.8) as:

$$\alpha(r) = \alpha_1 r^{N/2} + ... \tag{C.34}$$

$$\beta(r) = \frac{1}{N+1}(\omega T_0 - m)\alpha_1 r^{N/2+1} + ... \tag{C.35}$$

$$A(r) = 1 - \frac{\Lambda}{3}r^2 - 8\pi\omega T_0^2\alpha_1^2\frac{N}{N+1}r^N + ... \tag{C.36}$$

$$T(r) = T_0 + \sum_{k\geq 2 \text{ even}}^{N-2}\left(\frac{\Lambda}{3}\right)^{k/2}\frac{(k-1)!!}{k!!}T_0 r^k + \left(\left(\frac{\Lambda}{3}\right)^{N/2}\frac{(N-1)!!}{N!!}T_0 - 4\pi T_0^2\alpha_1^2\frac{1}{N+1}(2T_0\omega - m)\right)r^N + ... \tag{C.37}$$

More concisely, (C.37) can be expressed as

$$T(r) = T_0 + \sum_{k=1}^{N/2} \left(\frac{\Lambda}{3}\right)^k \frac{(2k-1)!!}{2k!!} T_0 r^{2k} - 4\pi T_0^2 \alpha_1^2 \frac{1}{N+1}(2T_0\omega - m) r^N + ... \tag{C.38}$$

Small r expansion for ED equations with non-zero cosmological constant and uniform matter background

In the presence of a uniform matter background, the ED equations are

$$rA' = 1 - A - \Lambda r^2 - 8\pi(N\omega T^2(\alpha^2 + \beta^2) + \rho), \tag{C.39}$$

$$2rA\frac{T'}{T} = A - 1 + \Lambda r^2 - 8\pi \left(N\omega T^2(\alpha^2 + \beta^2) - \frac{N^2\sigma}{r} T\alpha\beta - 8\pi N m T(\alpha^2 - \beta^2) + P \right), \tag{C.40}$$

while the Dirac equation components (C.1) and (C.2) remain the same. The calculation of the expansions is done as above, and most coefficients remain the same. At order r^2, (C.39) and (C.40) give

$$2A_2 r^2 = -A_2 r^2 - (\Lambda + 8\pi\rho) r^2, \tag{C.41}$$

$$4T_2 = (A_2 + (\Lambda - 8\pi P)) T_0. \tag{C.42}$$

This implies

$$A_2 = -\frac{1}{3}(\Lambda + 8\pi\rho), \tag{C.43}$$

$$T_2 = \frac{T_0}{6}(\Lambda - 4\pi(\rho + 3P)). \tag{C.44}$$

To calculate the recursive relation between T_n and T_{n-2}, we compute the equivalent of (C.23)

$$2r(nT_n r^{n-1} + A_2 r^2 T_{n-2}(n-2) r^{n-3}) = (A_2 + (\Lambda - 8\pi P)) T_{n-2}, \tag{C.45}$$

which yields

$$T_n = \frac{1}{3n}\left(\Lambda(n-1) + 8\pi\rho(n - \frac{5}{2} - \frac{3}{2}w)\right) T_{n-2}. \tag{C.46}$$

While the expansions for α and β remain equal to (C.34) and (C.35), the expansions for A and T are

$$A(r) = 1 - \frac{1}{3}(\Lambda + 8\pi\rho) - 8\pi\omega T_0^2 \alpha_1^2 \frac{N}{N+1} r^N + ... \tag{C.47}$$

$$T(r) = T_0 + \sum_{k=1}^{N/2} \left(\frac{1}{3}\right)^k \frac{(\Lambda(2k-1) + 4\pi\rho(4k-5-3w))!!}{2k!!} T_0 r^{2k}$$

$$- 4\pi T_0^2 \alpha_1^2 \frac{1}{N+1}(2T_0\omega - m) r^N + ... \tag{C.48}$$

Appendix D.

Construction of the unscaled solutions to the ED system

The numerical solutions that are obtained via the binary search algorithm cease to be sensible at some large radius r_f. This happens because the tuning of ω can only be carried out to finite precision. At r_f, the fermion fields usually diverge.

To compute the rescaling parameters l and τ, we need to construct functions that are valid for all radii, and not only between r_i and r_f. For $r < r_i$, we join the solutions computed by the numerical solver to the the Taylor expansions (3.1) - (3.4). At large r, the metric fields A and T approach the Schwarzchild-(anti-)de Sitter metric of (2.15) and (2.16). It is important that we join the numerical solutions to the asymptotic metric at a radius $r < r_f$, to avoid the imprecise behaviour around r_f. We attach A and T to the fitted Schwarzchild-(anti-)De Sitter metric, from which we extract the ADM mass.

For the fermion fields, the exponential decay of the evanescent zone is strong enough so that they drop to very small values (i.e., or order $1 \cdot 10^{-6}$). We approximate them to be zero at large r. Having constructed the unscaled solutions to the ED system, we proceed to compute the rescalings and to define the scaled solutions as detailed in Section 3.1.